

Dynamics of Willapa Bay, Washington: A Highly Unsteady, Partially Mixed Estuary

N. S. BANAS, B. M. HICKEY, AND P. MACCREADY

School of Oceanography, University of Washington, Seattle, Washington

J. A. NEWTON

*School of Oceanography, University of Washington, Seattle, and Environmental Assessment Program,
Washington State Department of Ecology, Olympia, Washington*

(Manuscript received 24 February 2003, in final form 4 May 2004)

ABSTRACT

Results from 3 yr of hydrographic time series are shown for Willapa Bay, Washington, a macrotidal, partially mixed estuary whose river and ocean end members are both highly variable. Fluctuating ocean conditions—alternations between wind-driven upwelling and downwelling, and intrusions of the buoyant Columbia River plume—are shown to force order-of-magnitude changes in salinity gradients on the event (2–10 day) scale. An effective horizontal diffusivity parameterizing all up-estuary salt flux is calculated as a function of riverflow: results show that Willapa's volume-integrated salt balance is almost always far from equilibrium. At very high riverflows (the top 15% of observations) the estuary loses salt, on average, while at all other riverflow levels it gains salt. Under summer, low-riverflow conditions, in fact, the effective diffusivity K is large enough to drive a net increase in salinity that is 3–6 times the seaward, river-driven salt flux. This diffusion process is amplified, not damped, by increased tidal forcing, contrary to the expectation for baroclinic exchange. Furthermore, K varies along the length of the estuary as $\sim 5\%$ of the rms tidal velocity times channel width, a scaling consistent with density-independent stirring by tidal residuals. To summarize Willapa's event- and seasonal-scale variability, a simple diagnostic parameter space for unsteady estuarine salt balances is presented, a generalization from the Hansen and Rattray steady-state scheme.

1. Introduction

This paper examines the net fluxes of salt in and out of Willapa Bay, Washington, on event (2–10 day) and seasonal time scales. Willapa is a coastal-plain estuary connected to a highly active eastern boundary ocean, the northern reach of the California Current System (Hickey 1989). The interest of salt dynamics in this estuary is on one level regional and ultimately ecological, while at the same time is tied to a general, theoretical concern: the often-neglected role of time-dependence in estuarine dynamics and classification.

Analytical theories of estuarine circulation overwhelmingly rely upon the assumption of a steady state to reach tractable solutions. The classical core of this field is the analytical solution of Hansen and Rattray (1965), hereinafter HR65, and the closely related diagnostic scheme of Hansen and Rattray (1966), hereinafter HR66. The HR66 scheme describes estuaries through a steady-state balance of three salt fluxes: down-estuary advection of salt by the mean flow, up-estuary

return of salt by the vertical gravitational circulation, and an up-estuary “diffusive” flux, representing all other exchange, which closes the balance. The generalization of this theory to include time dependence (MacCready 1999) is embryonic, although in more observational contexts, as we review below, time-dependent river, ocean, and atmospheric forcing have all received wide attention.

Order-of-magnitude changes in river input are common on not only seasonal but few-day time scales in many systems (e.g., Uncles and Peterson 1996; Simpson et al. 2001). Studies of the estuarine response to changing riverflow, in terms of both their time scale (Kranenburg 1986; MacCready 1999) and magnitude (Officer and Kester 1991; Gibson and Najjar 2000; Monismith et al. 2002) occupy much of the literature.

Both remote and local wind forcing (“remote” refers to offshore processes, while “local” refers to wind over the estuary itself) typically vary on both seasonal and event timescales. Remote wind is generally taken to affect estuaries through sea level setup and setdown, which drive secondary or pumping circulations (Wang and Elliott 1978; Walters 1982; Wang et al. 1997). It also can control water properties through coastal upwelling and downwelling, as discussed more below. Lo-

Corresponding author address: Neil S. Banas, School of Oceanography, Box 355351, University of Washington, Seattle, WA 98195.
E-mail: neil@ocean.washington.edu

cal wind can drive time-variable lateral circulations within an estuary, particularly over variable topography (Wong and Moses-Hall 1998; Geyer 1997).

Spring–neap variations in tidal amplitude can force large changes in estuarine circulation, both by directly modulating tidal residual flows (Kjerfve 1986) and by changing the dynamics of vertical mixing, which in turn controls the baroclinic circulation (Linden and Simpson 1988; Jay and Smith 1990; Park and Kuo 1996). Variations in oceanic water properties can also be important. In eastern boundary systems with narrow continental shelves and fluctuating wind forcing, variations in the strength of upwelling can cause salinity changes of several practical salinity units (psu) on time scales as short as 1–2 days (Hickey 1989). Upwelling and downwelling are the dominant mode of ocean end-member variability in Willapa Bay (Hickey et al. 2002).

Large, external sources of freshwater can also impinge on smaller estuaries nearby (e.g., the Delaware River, Wong and Lu 1994; the Mississippi, Wiseman et al. 1990). During downwelling periods the Columbia River plume enters both Willapa Bay and Grays Harbor to the north (Roegner et al. 2002; Hickey and Banas 2003). Small outer-coast estuaries downstream of a large river plume may even be thought of as a kind of tributary estuary (i.e., a small system contained within a larger one), which frequently are controlled by external water-property variations (Pritchard and Bunce 1959; Pritchard and Carpenter 1960; Schroeder et al. 1992). External water-property variations can themselves affect the mean baroclinic circulation, by intensifying or weakening along-channel density differences (Duxbury 1979; Monteiro and Largier 1999; Hickey et al. 2002).

Event-scale dynamical coupling between ocean and estuary is of particular interest in Willapa Bay and the rest of the Pacific Northwest coast, because in this region upwelling, not riverflow, is the primary source of estuarine nutrients and primary production (Roegner et al. 2002; Hickey and Banas 2003). The rate of ocean–estuary exchange is thus a very basic control on Willapa’s ecology (Roegner et al. 2002). This is likely to be true as well in the other small coastal-plain estuaries of the Pacific Northwest (see Emmett et al. 2000). With the notable exception of the Columbia River, these estuaries have received almost no oceanographic attention beyond the few studies cited here. They inhabit a coherent regime of forcing very different from other North American coasts (Hickey and Banas 2003)—large tidal ranges, strong variations in ocean water properties on all time scales, and highly seasonal riverflow that is lowest during the summer growing season. These estuaries appear to be more similar to many on the north coast of Europe (the Volkerak, Dronkers and van de Kreeke 1986; Wadden Sea embayments, Zimmerman 1976) and the British Isles (the Mersey, Bowden and Gilligan 1971; the Conwy, Simpson et al. 2001) than to other North American systems.

This paper describes three years of observations in

Willapa Bay, in the context of the subtidal, volume-averaged salt balance. Section 2 describes the study area and the range of hydrographic conditions observed on seasonal and event scales: this is the most detailed climatology of a Pacific Northwest coast estuary presented to date. In section 3 we derive a working form of the salt balance and evaluate the terms as a function of riverflow. Two key results emerge from this analysis, which we explore in more detail in the remaining sections. First, we will show that a riverflow-independent, diffusive salt flux dominates over the river-driven gravitational circulation in all but the top 25% of riverflow conditions: in section 4 we explain this diffusion process in terms of lateral stirring by tidal residuals. Second, we will show that for much of the year in Willapa, the three terms in the HR66 salt budget do not balance even to order of magnitude at any time scale from days to months: a diagnostic scheme appropriate for such time-dependent systems is the subject of section 5.

2. The seasonal cycle in Willapa Bay

a. Study area

A map of Willapa Bay is shown in Fig. 1. Willapa is the first embayment north of the Columbia River estuary on the Washington coast. It is comparable in depth and volume to Grays Harbor, immediately north of it, and South San Francisco Bay, and several times as large as the many small estuaries along the coast of Oregon (Hickey and Banas 2003). The estuarine geography of this coast is reviewed by Emmett et al. (2000), and its oceanography reviewed by Hickey (1989) and Hickey and Banas (2003).

Willapa consists of three main channels 10–20 m deep surrounded by extensive tidal flats. One channel stretches east from the mouth; Stanley Channel is longer and extends south from the mouth to the Naselle River; a third channel branches southwest off Stanley Channel into a broad intertidal region with virtually no river input. In the analysis that follows, we have confined our attention to Stanley Channel so that we can schematize the estuary as a single channel with an ocean at one end and a river at the other. The Naselle River, at the head of Stanley Channel, provides roughly one-fifth of the total freshwater input into the bay; the largest rivers are the North and the Willapa, both closer to the mouth. The effect of this river configuration is considered where appropriate. Area and depth profiles of Stanley channel are shown in Fig. 2.

The tide is mixed-semidiurnal, and the mean daily tidal range, which varies by ~20% over the length of the estuary and ~50% over the spring–neap cycle, is 2.7 m. In the *thalweg* at the mouth, the rms tidal velocity is 0.7–1.0 m s⁻¹. Almost one-half of the surface area of the estuary lies in the intertidal zone (160 km² out of 350 km²; Andrews 1965), and ~50% of the volume does as well: this extremely large intertidal fraction is

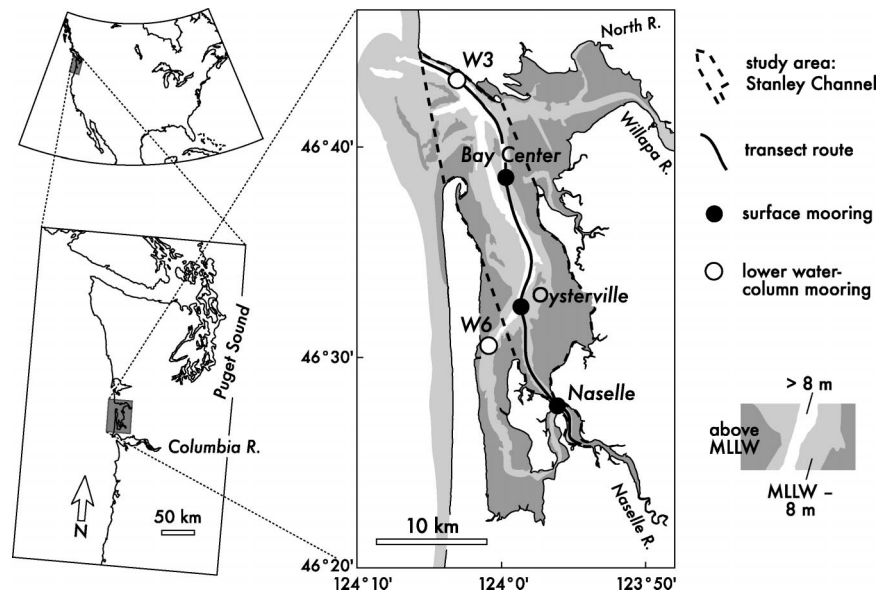


FIG. 1. Maps of Willapa Bay, the Pacific Northwest coast, and North America. Mooring locations and the axial transect route are indicated.

typical on the Pacific Northwest coast, though unusual among other North American outercoast estuaries (Hickey and Banas 2003).

b. Data sources

This study uses data from August 1997 to February 2001 from five time series stations and from 54 hydrographic transects of Stanley Channel during that period (Fig. 2). Station locations are shown in Fig. 1. Bay Center, Oysterville, and Naselle are piling-mounted SeaBird CT packages that follow sea level 1 m below the surface. The locations W3 and W6 are taut-wire moorings instrumented at ~ 8 m depth, in the mid-to-lower water column. Salinity data at W3 are from a SeaBird Microcat CT for one deployment and from an Aanderaa current meter carrying a CT cell for the others. The salinity record at W6 is short (6 months) and has been excluded from the analysis. Velocities at W3 and W6 from InterOcean S4 current meters are used to estimate tidal current amplitude.

These station salinity data, while well-resolved in time (observations every 15–30 min), do not resolve vertical or lateral salinity variations. To provide a record of stratification we use hydrographic transects of the main channel, which were conducted at least monthly from small boats with SeaBird 19 and 25 CTDs. Many of these surveys were coordinated with mooring maintenance and took 4 h or more to cover Stanley Channel. As a result, because of tidal aliasing, we do not use transect data in the calculation of subtidal time series (section 3b). Bank-to-channel variation was explored through ~ 10 day-long series of CTD surveys (see Hickey and Banas 2003). These data are used here simply

to confirm the assumption (section 3c) that the total salt storage of the estuary is well-indexed by the salinity of the main channel.

Most gaps in the station records (Fig. 2) indicate periods in which salinity measurements were biased or degraded by biofouling, rather than gaps in deployment. We report only periods in which salinities are consistent between station and transect observations. Station temperature records are much more continuous.

Estimates of riverflow are derived from U.S. Geological Survey (USGS) gauges 12013500 and 12010000 on the Willapa and Naselle rivers. Only 19% of Willapa's watershed lies above these gauges: to calculate bay-total flow, we multiply the gauged flows by the inverse of this fraction (Lincoln 1977). The resulting estimate is consistent with the annual mean value reported by the National Oceanic and Atmospheric Administration/Environmental Protection Agency (NOAA/EPA 1991) to 20%.

The bathymetry used in calculating channel areas and volumes was provided by the Army Corps of Engineers, Seattle District, who resurveyed most of the subtidal area of Willapa in 1998 (Kraus 2000). We make use also of the NOAA tidal-height predictions for Toke Point and Nahcotta, stations 9440910 and 9440747. Wind data are from the National Centers for Environmental Prediction (NCEP)–National Center for Atmospheric Research (NCAR) Reanalysis project (Kalnay et al. 1996).

c. The seasonal cycle

Here we describe variations in Willapa's hydrography over a typical year, August 1999–August 2000. The

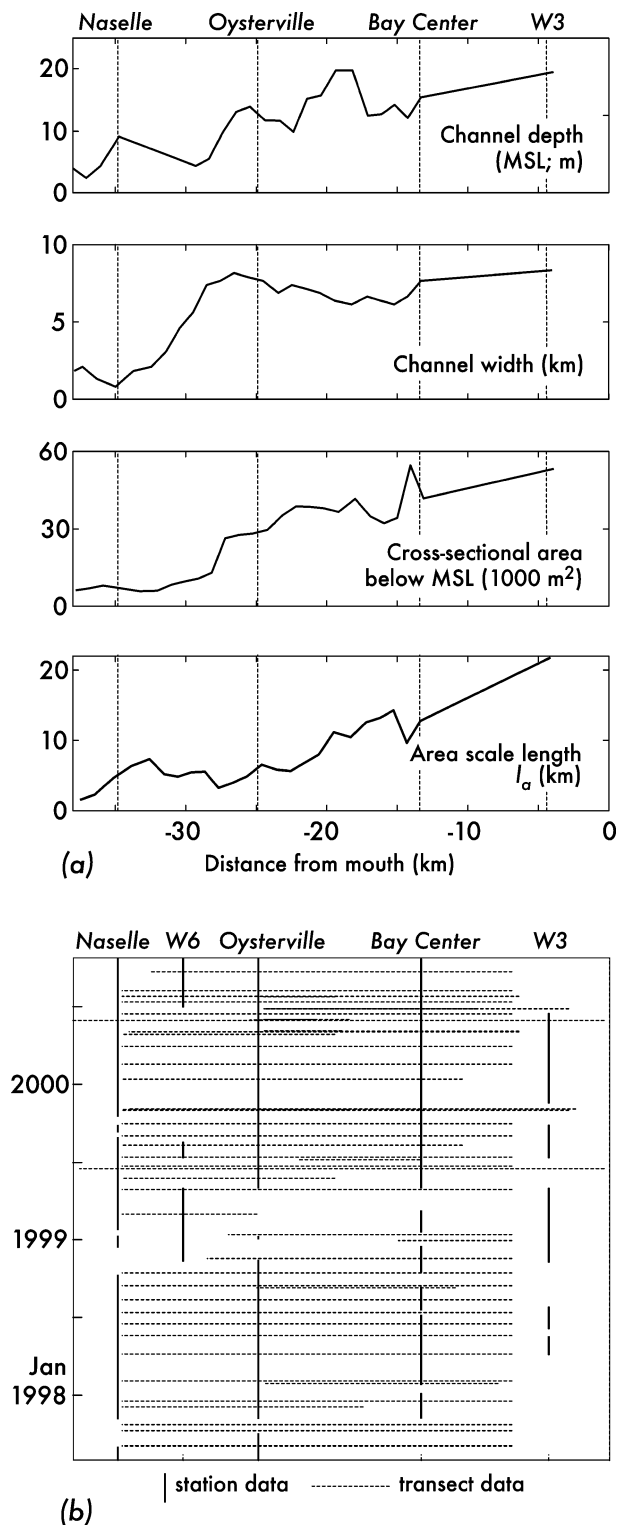


FIG. 2. (a) Depth of the main channel, channel width (measured shore-to-shore), cross-sectional area, and the scale length l_a (upstream volume divided by cross-sectional area) along Stanley Channel from the Naselle River to the estuary mouth. (b) Data coverage of Stanley Channel, Aug 1997–Feb 2001: vertical lines indicate station time series; horizontal lines show main-channel CTD transects.

large-scale winds in this region (Fig. 3a) are predominantly southward (upwelling favorable) during the summer and during breaks of fair weather at other times of year, and northward (downwelling favorable) during the winter and foul-weather events (Hickey 1989). There are event-scale reversals in the winds during almost every month of the year. Riverflow (Fig. 3b) is likewise intermittent on the event scale and varies by a factor of several hundred between the late summer low-flow period and the largest winter flows. Note that river and ocean forcing of the estuary cannot be separated statistically as distinct modes of variation: riverflow into Willapa reflects recent local rainfall rather than snowmelt, and rainfall in this region, like coastal upwelling and downwelling, is well correlated with large-scale winds (Figs. 3a,b).

Shown in Figs. 3c–h are six salinity sections along Stanley Channel, which we now consider in turn.

At the end of September (Fig. 3c), riverflows have been negligible ($\sim 10 \text{ m}^3 \text{ s}^{-1}$) and upwelling conditions predominant for several months. There is very weak buoyancy input into the bay from both rivers and ocean, and salinities are high even at the mouth of the Naselle River. Vertical and axial salinity gradients are simultaneously weak. A few days after the first substantial rain of the season (Fig. 3d), salinities are markedly lower near the head of the channel, producing locally strong salinity gradients. Most of the channel remains relatively well mixed, though salinities throughout are lower than in the 30 September transect.

During heavy, sustained winter riverflows (Fig. 3e) the entire estuary stratifies dramatically, concomitant with a large salinity difference between mouth and head. The most seaward reach of the estuary was not surveyed on this transect because of sea conditions, but salinities near the mouth appear to be ~ 10 psu lower than during the summer upwelling period. On 3 May (Fig. 3f) the salinity at the mouth is likewise only 21 psu, even though local riverflow has slackened. During late spring, the Columbia River, 50 km south of the Willapa Bay entrance, is running at its highest because of snowmelt from the inland mountains. Under downwelling winds, the plume from the Columbia flows north against the coast and enters both Willapa and Grays Harbor. Under this forcing, in which a buoyant water mass enters the mouth at all depths under a strong tidal flow, the estuarine water column actively mixes and tends toward extremely low horizontal and vertical density gradients. The axial gradient can in fact reverse for sustained periods: the transect in Fig. 3f shows one such reversal over ~ 10 km in the middle of the estuary. The dynamics and evolution of these plume intrusions, which are common in winter and spring, are considered in more detail by Hickey and Banas (2003).

During late spring and early summer, the coastal wind direction is intermittent and plume-intrusion events alternate with upwelling events (Fig. 3g). Spring upwelling typically brings the strongest head-to-mouth sa-

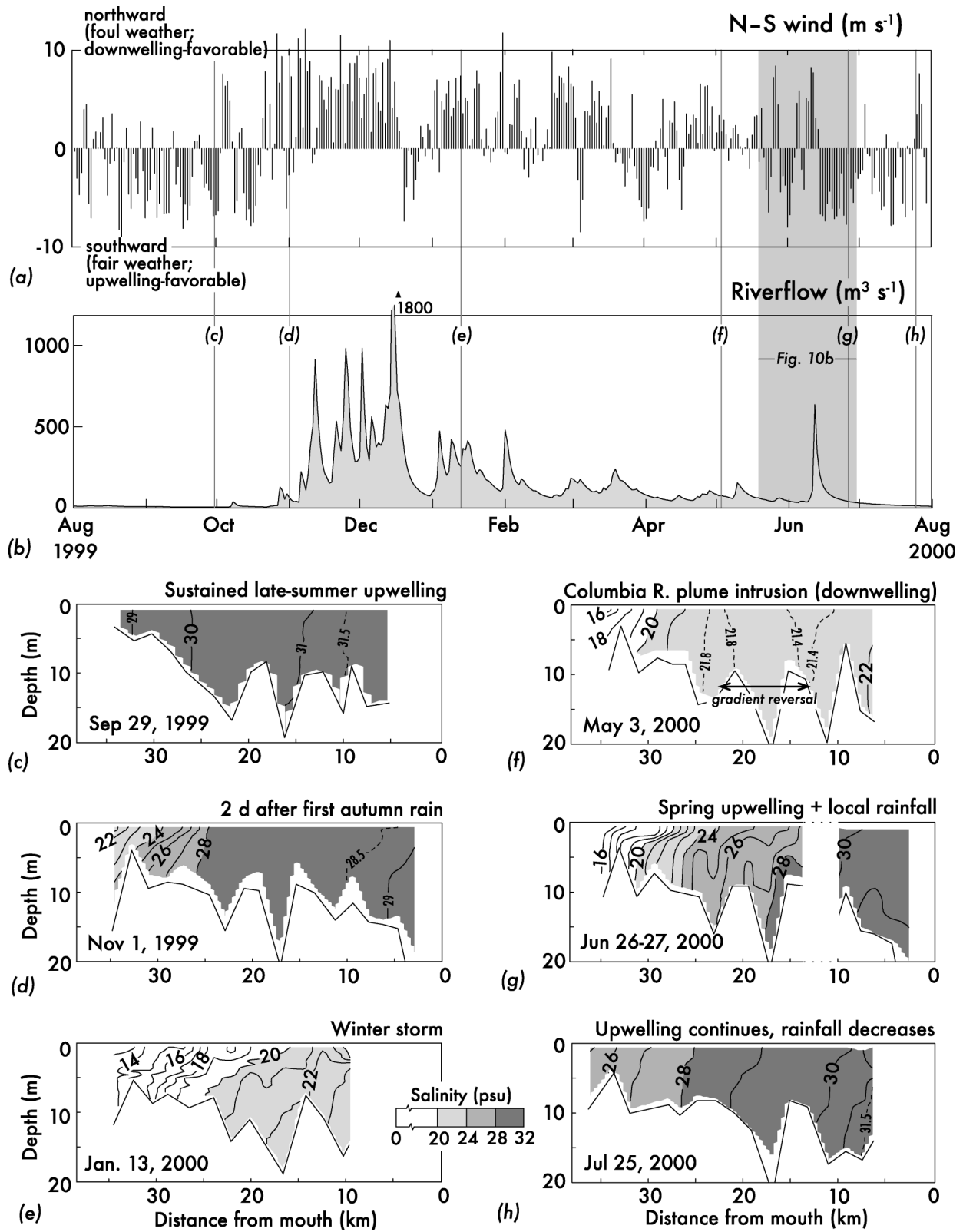


FIG. 3. (a), (b) Meteorological forcing and (c)–(h) six axial salinity transects for the year Aug 1999–Aug 2000. Gray vertical lines in (a) and (b) indicate times of the six transects and are indexed to the panels below. The time period expanded in Fig. 10b is shaded as well. The transect route is shown in Fig. 1.

linity differences of the year. Finally, as riverflow slackens over the course of the summer (Fig. 3h), salinity at the head increases, and vertical and horizontal gradients weaken. The bay thus gradually returns to the nearly-well-mixed conditions shown in Fig. 3c. Event-scale wind reversals interrupt this trend (Fig. 3a), though not as dramatically as during early summer.

As these six snapshots suggest, over the course of a year Willapa Bay cycles or weaves over an enormous range of the possible hydrographic states of a partially mixed estuary. Because ocean and river forcing are both so variable—and because the impact of event-scale ocean variability is not confined to the mouth, but rather penetrates through most of the volume of the bay—no monotonic relationship exists between either ocean salinity or riverflow and estuarine salinity gradients. Nevertheless, we can estimate the relative roles of time dependence, riverflow, gravitational circulation, and other salt-loading mechanisms using a simplified form of the volume-integrated salt balance. This calculation is the subject of the next section.

3. The salt balance

a. Theory

We will begin by deriving our working form of the salt balance; in section 3b we describe our methods for calculating the terms in this balance from data, and in section 3c and 3d we use these tools to describe the dynamics of Willapa Bay across forcing conditions.

We start with a general budget equation for salt, in which we have averaged over a cross section of the estuary (denoted by an overbar), averaged as well over the tidal cycle (angle brackets), and finally integrated in the axial (x) direction from far upstream where salt flux is zero ($x = -\infty$) to x :

$$\frac{\partial}{\partial t} \int_{-\infty}^x \langle a\bar{s} \rangle dx + \langle a\bar{u}\bar{s} \rangle = 0. \quad (3.1)$$

Here t is time, s is salinity, u is axial velocity, and a is cross-sectional area. The first term describes subtidal changes in total salt storage upstream of x on subtidal time scales, and the second denotes total salt flux through the cross section at x . The integral in the first term can be written more simply as $V\bar{s}$, where V is mean volume upstream of x and \bar{s} the mean salinity over that volume. We also can define an area length scale $l_a \equiv V\langle a \rangle^{-1}$ so that (3.1) becomes

$$l_a \frac{\partial \bar{s}}{\partial t} + \frac{1}{\langle a \rangle} \langle a\bar{u}\bar{s} \rangle = 0. \quad (3.2)$$

Values of l_a along Stanley Channel are given in Fig. 2. Note that we have assumed a term on the left-hand side involving $\partial V/\partial t$, and thus wind-driven sea level setup and setdown, to be small. In other estuaries this term may in fact be more important than the $\partial \bar{s}/\partial t$ term, but Hickey et al. (2002) found that the large-scale winds

affect circulation in Willapa primarily through upwelling- and downwelling-related salinity changes and not barotropic volume changes.

All the mechanisms that move salt up- and downstream are contained within the total flux term $\langle a\bar{u}\bar{s} \rangle$. A common approach, beginning with HR65, has been to decompose this flux into three terms as follows:

$$\langle a\bar{u}\bar{s} \rangle = \langle a \rangle \left(\langle \bar{u} \rangle \langle \bar{s} \rangle + \langle \bar{u}'s' \rangle - K \frac{\partial \langle \bar{s} \rangle}{\partial x} \right). \quad (3.3)$$

Here u' and s' are defined as spatial fluctuations around \bar{u} and \bar{s} such that $\overline{u'} \equiv \overline{s'} \equiv 0$, and K is a horizontal diffusivity. The first term on the right-hand side represents seaward advection of salt by the mean flow: \bar{u} is related to riverflow Q by

$$\langle Q \rangle = \langle a\bar{u} \rangle, \quad (3.4)$$

where again we have ignored sea level setup- and setdown-driven volume changes (an assumption that may not be valid if the salt balance is to be evaluated not in long averages, as we do below, but on the event scale). We will refer to $\langle \bar{u} \rangle \langle \bar{s} \rangle$ as the “river” or “river-flushing” term. The second term in (3.3) describes correlations between the mean vertical structures of velocity and salinity: in the HR65 theory this correlation describes a steady vertical exchange flow or gravitational circulation. Last, the third, or diffusion, term, parameterizes all remaining correlations between a , u , and s : Stokes drift (tidal correlations between a and u), “tidal trapping” in side channels or on banks (tidal correlations between u and s), stirring by tidal residuals (lateral correlations between $\langle u \rangle$ and $\langle s \rangle$), and several other terms. For more detailed discussion of these terms, see Fischer (1976); for full empirical salt-flux decompositions in individual estuaries, see Hughes and Rattray (1980), Winterwerp (1983), Lewis and Lewis (1983), and Dronkers and van de Kreeke (1986).

In the steady case ($\partial \bar{s}/\partial t = 0$), (3.2), (3.3), and (3.4) become the classical HR66 salt balance:

$$\frac{Q}{a} \bar{s} = -\overline{u's'} + K \frac{\partial \bar{s}}{\partial x}. \quad (3.5)$$

We have dropped the angle brackets for brevity. In this case, total upstream salt flux (the right-hand side) exactly balances river-flushing, and is partitioned between a steady gravitational circulation and an undifferentiated diffusion process. A classification parameter v , the diffusive fraction of upstream salt flux, can then be defined as

$$v \equiv \frac{K \frac{\partial \bar{s}}{\partial x}}{\overline{u's'} + K \frac{\partial \bar{s}}{\partial x}}. \quad (3.6)$$

When $v = 0$ river-flushing balances gravitational circulation, and when $v = 1$ river-flushing balances diffusion. A more general scheme that diagnoses the full

unsteady salt balance as ν diagnoses the steady HR66 balance is the subject of section 5.

In an estuary where stratification and shear vary significantly over the tidal cycle (Jay and Smith 1988; Stacey et al. 2001) or vary laterally because of Coriolis or topography (Li and O'Donnell 1997), it may be misleading to equate the gravitational circulation with the mean quantity $\overline{u's'}$. Since in the present study we lack the data to decompose $\langle \overline{u's'} \rangle$ with enough detail to resolve these effects, we will use a formulation even simpler than the HR65 decomposition (3.3):

$$\langle \overline{u's'} \rangle = \langle a \rangle \left(\langle \overline{u} \rangle \langle \overline{s'} \rangle + K_{\text{tot}} \frac{\partial \langle \overline{s'} \rangle}{\partial x} \right). \quad (3.7)$$

Here K_{tot} is a total effective diffusivity, which parameterizes all upstream salt-flux mechanisms, including the gravitational circulation. Combining (3.7) with (3.2) and (3.4) yields the general unsteady salt balance

$$l_a \frac{\partial \overline{s}}{\partial t} + \frac{Q}{a} \overline{s} = K_{\text{tot}} \frac{\partial \overline{s}}{\partial x}, \quad (3.8)$$

where again we have dropped the angle brackets. We can diagnose the unsteadiness of the salt balance by comparing K_{tot} with an equilibrium value $K_{\text{tot}}^{\text{eq}}$, defined by

$$\frac{Q}{a} \overline{s} = K_{\text{tot}}^{\text{eq}} \frac{\partial \overline{s}}{\partial x}. \quad (3.9)$$

When $K_{\text{tot}} < K_{\text{tot}}^{\text{eq}}$, river-flushing exceeds upstream salt flux and the estuary loses salt; when $K_{\text{tot}} > K_{\text{tot}}^{\text{eq}}$, the estuary gains salt. We will evaluate K_{tot} and $K_{\text{tot}}^{\text{eq}}$ for Willapa in section 3c.

This total-diffusivity approach, with and without the assumption of a steady state, has been used in a number of studies (e.g., Uncles and Stephens 1990; Monismith et al. 2002; Lewis and Uncles 2003). It is convenient where data are sparse, but it has the drawback of leaving the dynamics of upstream salt flux ambiguous. In section 3d, we will describe an empirical decomposition of K_{tot} that to some extent allows us to recover the dynamical information in the HR66 formulation.

b. Calculation methods

Before continuing with the K_{tot} calculation, in this section we discuss the methods by which the spatially integrated quantities \overline{s} , $\partial \overline{s} / \partial t$, and $\partial \overline{s} / \partial x$ are estimated from our point measurements.

For simplicity we let station salinities represent \overline{s} without adjustment: i.e., we ignore vertical and lateral salinity variations. (The error associated with this and our other approximations is discussed below.) We calculate $\partial \overline{s} / \partial x$ not as a difference between stations, but as a point measurement at each station, taking advantage of the fact that over a tidal cycle each station samples a full tidal excursion of the channel. Dividing the difference between end-of-flood and end-of-ebb salinity by the tidal excursion gives one value of $\partial \overline{s} / \partial x$ for each

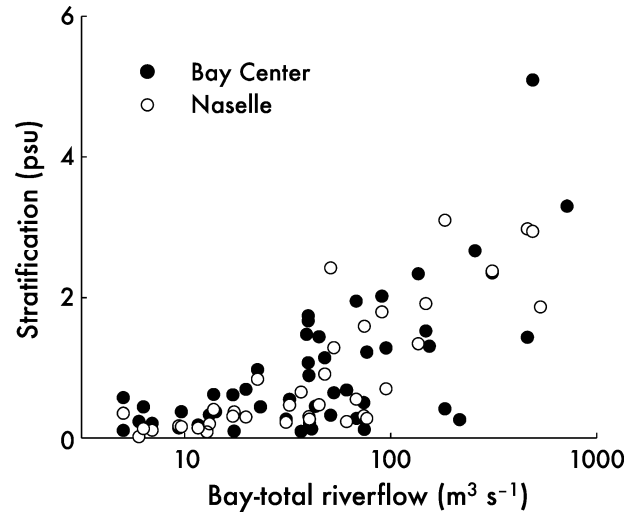


FIG. 4. Surface-to-bottom salinity difference at Bay Center and Naselle from transect data, shown as a function of riverflow. Data are instantaneous and therefore tidally aliased.

tidal cycle, and low-pass-filtering this discrete series gives a continuous subtidal time series. This method, unlike differencing between stations, gives a truly local measure of $\partial \overline{s} / \partial x$ and is unaffected by gaps in coverage at other stations. Last, to evaluate $\partial \overline{s} / \partial t$ we calculate total upstream salt storage $V \overline{s}$ as a linear combination of landward station salinities; for example, at Bay Center,

$$\begin{aligned} \frac{\partial}{\partial t} (V \overline{s})_{\text{Bay Ctr}} \\ = \frac{\partial}{\partial t} (0.25 s_{\text{Bay Ctr}} + 0.20 s_{\text{Oyst}} + 0.06 s_{\text{Naselle}}) \times 10^9 \text{ m}^3. \end{aligned} \quad (3.10)$$

The coefficients are calculated from total volume below MSL between each pair of stations.

We estimate from axial and lateral transect data that at Bay Center, the total uncertainty in \overline{s} associated with unresolved salinity variations in all three dimensions is only $\sim 10\%$. This level is set by the maximum discrepancy between measured (surface) salinity and vertical-mean salinity taking into account stratification (Fig. 4). Errors from lateral salinity variations are less than 10%: differential tidal advection has been seen to create bank-to-channel salinity variations near Bay Center of several practical salinity units (Hickey and Banas 2003) but these gradients are only strong over very shallow banks, where their volume-integrated effect is smallest. Station spacing in the axial direction is comparable to the tidal excursion and accordingly appears sufficient to resolve subtidal axial salinity variations throughout the bay.

A potentially much larger—and harder to quantify—source of uncertainty is the proximity of W3 and Oystererville to the subestuaries outside Stanley Channel. In particular, 80% of riverflow into the bay enters between

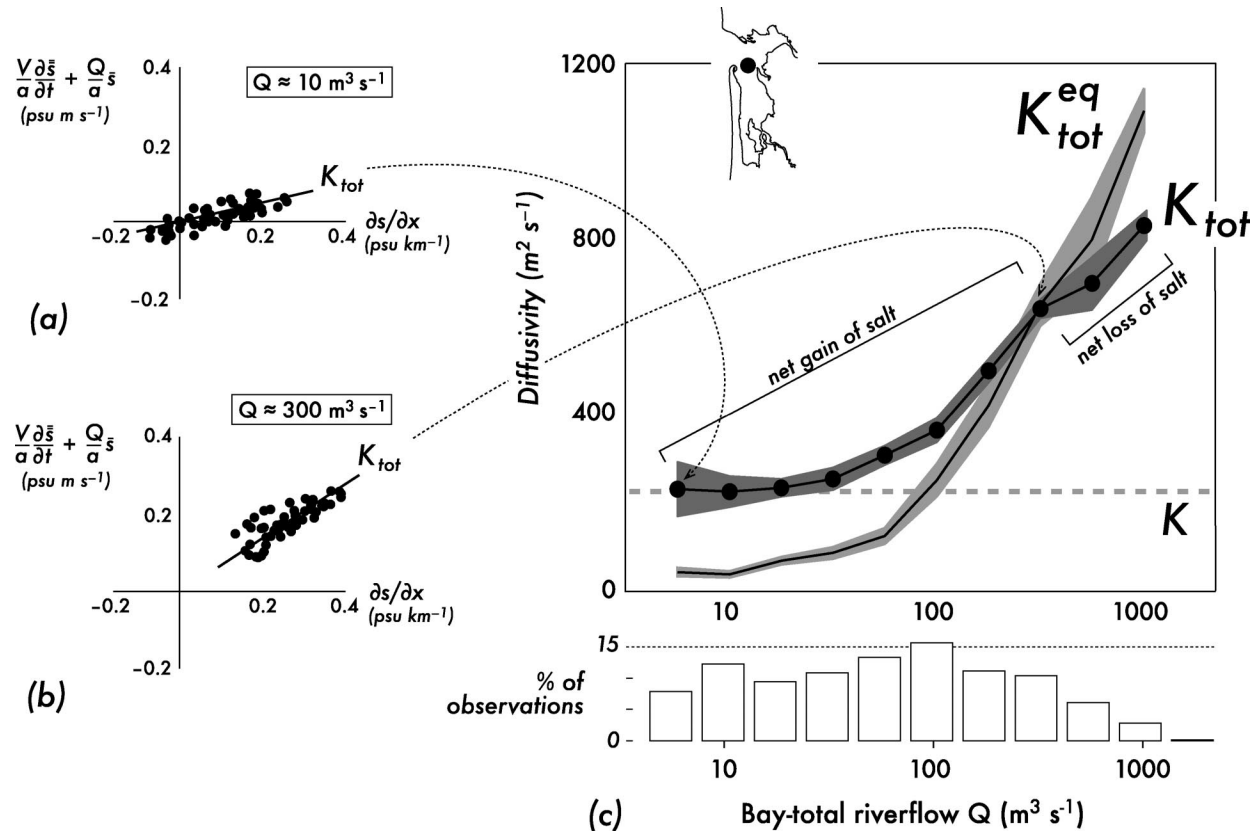


FIG. 5. (a), (b) Regression between the left-hand side of (3.8)—the time-change and river-flushing terms—and axial salinity gradient at Bay Center for two riverflow bins. The slope of the regression is the effective diffusivity K_{tot} . (c) The diffusivity K_{tot} calculated as in (a) and (b) for all riverflow bins, along with the equilibrium value $K_{\text{tot}}^{\text{eq}}$, calculated by analogous regressions between the river term alone and $\partial\bar{s}/\partial x$ [(3.9)]. Shaded areas give 95% confidence limits. The dashed horizontal line shows the value of the low-flow diffusivity K as defined in section 3d. A histogram of riverflow values over the three-year study period is also shown.

Bay Center and W3, but the lateral distribution of this freshwater around W3 and the mouth of the bay is unclear: sea conditions make Willapa's entrance shoals impossible to survey from a small boat. As a result, in the analysis that follows, we evaluate the salt balance at Bay Center, where the geometry is simplest and our data coverage best, in the most detail.

c. Total effective diffusivity

We now have estimates of every quantity in (3.8) except for K_{tot} and can in principle solve for K_{tot} as a continuous subtidal time series. In practice, it is more statistically robust to calculate K_{tot} in an ensemble average, as the mean slope between the left-hand side of (3.8) and $\partial\bar{s}/\partial x$ for some set of measurements. We will start by binning observations by bay-total riverflow, as a proxy for meteorological forcing in general.

Results of the K_{tot} calculation for Bay Center are shown in Fig. 5. Individual data points for two riverflow bins are shown in Figs. 5a and 5b, and ensemble averages for all bins are shown in Fig. 5c along with 95% confidence limits. These confidence limits are generally

larger than the observational uncertainties estimated above: they thus appear to represent not error but real, ocean-forced variability within each riverflow bin. Data have been Butterworth-filtered with a cutoff frequency of $(10 \text{ days})^{-1}$, to average over the mean propagation time for ocean signals from the mouth to the head at Naselle (see section 4c). Shorter and longer filter periods change the magnitude of the variance within each riverflow bin but have a statistically insignificant effect on K_{tot} itself. This is one validation of the appropriateness of the total-diffusivity model.

K_{tot} increases with riverflow Q from $240 \text{ m}^2 \text{ s}^{-1}$ at very low flows to $840 \text{ m}^2 \text{ s}^{-1}$ at high flows: a change of a factor of 3.5. In comparison, the equilibrium value $K_{\text{tot}}^{\text{eq}}$ increases by more than a factor of 20 over the same riverflow range, from 50 to $1100 \text{ m}^2 \text{ s}^{-1}$. Willapa is thus far from equilibrium over nearly all flow conditions. For $Q < 300 \text{ m}^3 \text{ s}^{-1}$ (85% of observations), upstream salt flux exceeds river-flushing ($K_{\text{tot}} > K_{\text{tot}}^{\text{eq}}$) and the estuary gains salt. This is true on average: it is not necessarily true during individual, transient, ocean-forced events like Columbia plume intrusions. During high winter flows above $300 \text{ m}^3 \text{ s}^{-1}$, on average the river-

flushing term dominates ($K_{\text{tot}} < K_{\text{tot}}^{\text{eq}}$) and the estuary loses salt. Integrated over a full seasonal cycle, the salt budget does appear to balance: the mean K_{tot} and $K_{\text{tot}}^{\text{eq}}$ for the 1-yr period shown in Fig. 3 agree, perhaps coincidentally, within 2% (not shown).

d. Decomposition of upstream salt flux

In low-flow conditions, the difference between K_{tot} and $K_{\text{tot}}^{\text{eq}}$ is actually many times larger than $K_{\text{tot}}^{\text{eq}}$ itself (Fig. 5). This is only possible if the river term in (3.8) is negligible and the dominant balance is between the K_{tot} term and the time-change term, i.e., an unsteady diffusion process independent of riverflow. Stanley Channel thus appears more like a lagoon or riverless tidal embayment than like a true estuary during the summer low-flow period.

These simplified low-flow-period dynamics suggest an empirical division of up-estuary salt flux into river-driven and river-independent parts, analogous to the HR66 partitioning between river-driven gravitational circulation and “true” diffusion. We can write this as $K_{\text{tot}} \equiv K_{\text{gc}} + K$, where K is defined as the “baseline” or low-riverflow limit of K_{tot} (the dashed line in Fig. 5). The salt balance (3.8) then becomes

$$l_a \frac{\partial \bar{s}}{\partial t} + \frac{Q}{a} \bar{s} = K_{\text{gc}} \frac{\partial \bar{s}}{\partial x} + K \frac{\partial \bar{s}}{\partial x}. \quad (3.11)$$

The K_{gc} term is analogous to, but more general than, the $u's'$ in the HR66 formulation (3.5). More precisely, K_{gc} represents both the mean gravitational circulation at a given riverflow level and all nonlinear coupling between this gravitational circulation and diffusive exchange. K , the “true” diffusivity, represents a combination of tidal exchange (lateral stirring, trapping, Stokes drift), local-wind-driven processes, and modulations of the mean gravitational circulation by ocean density fluctuations (“baroclinic coupling”; Hickey et al. 2002).

The purpose of this decomposition is to isolate K so that its dependence on forcing can be examined, and a dynamical explanation obtained for the high, unequibrated rate at which Willapa loads seawater during low-flow conditions. In section 4 we will demonstrate that K is primarily a tide-driven, rather than baroclinic, process, and present a scaling that explains its variation over the length of Stanley Channel.

4. Tidal diffusion in low-flow conditions

a. Calculation of K

We begin by calculating K for all stations. Instead of repeating the full determination of $K_{\text{tot}}(Q)$ at every station besides Bay Center—data gaps and the geometric complexity discussed in section 3b make this difficult—we will use a simpler method. By definition, as $Q \rightarrow 0$, (3.8) approaches the diffusive limit

$$l_a \frac{\partial \bar{s}}{\partial t} = K \frac{\partial \bar{s}}{\partial x}. \quad (4.1)$$

Thus K can be calculated as the slope between the time-change term and $\partial \bar{s} / \partial x$ in the average over all low-flow conditions. “Low flows” are those for which the neglected river term is smaller than the standard deviation of the time-change term around its correlation with $\partial \bar{s} / \partial x$, and thus by definition well-contained within 95% confidence limits. To err on the side of an over-strict definition of low flows, we compute this threshold using bay-total riverflow for Q . At Naselle, salinity variance in summer is so small that even if we take Q to be Naselle flow alone, our low-flow definition excludes the entire record; results are given for Naselle riverflows $< 2 \text{ m}^3 \text{ s}^{-1}$.

Results are shown in Fig. 6 for all four stations. As in section 3, the data have been filtered with a cutoff frequency of $(10 \text{ days})^{-1}$. Mean values of K decrease from $710 \text{ m}^2 \text{ s}^{-1}$ at W3 to $20 \text{ m}^2 \text{ s}^{-1}$ at Naselle. The estimate at Naselle is not different from zero at the 95% confidence level, but it is a stable result, $\geq 20 \text{ m}^2 \text{ s}^{-1}$ regardless of the choice of filter timescale or riverflow threshold. The estimate at Bay Center calculated by this method agrees within confidence limits with the baseline K_{tot} shown in Fig. 5.

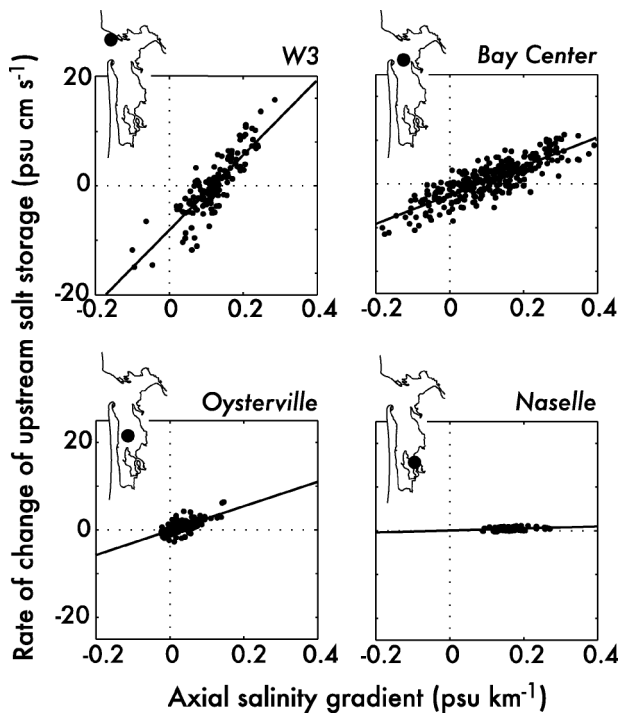
A number of factors presumably contribute to the scatter of individual events around the long-term mean: baroclinic ocean-estuary coupling, the small but non-zero river-driven salt fluxes permitted under our definition of “low flows,” spring-neap variations in tidal stirring (section 4c), lateral circulations driven by local wind, and non-Fickian tidal dispersion mechanisms (i.e., tidal salt fluxes not proportional to $\partial \bar{s} / \partial x$; Ridderinkhof and Zimmerman 1992; McCarthy 1993). For many individual events, the net salt flux explained by the constant-diffusivity regression is smaller than the salt flux it does not explain.

Nevertheless, a constant diffusivity explains one-half or more of the variance in 10-day and longer-scale salt fluxes everywhere except the river mouth itself (at W3 and Bay Center, the regressions in Fig. 6 have $r^2 = 0.7$; at Oysterville, $r^2 = 0.5$). In the sections that follow we examine the physical meaning of this very simple salt-flux parameterization.

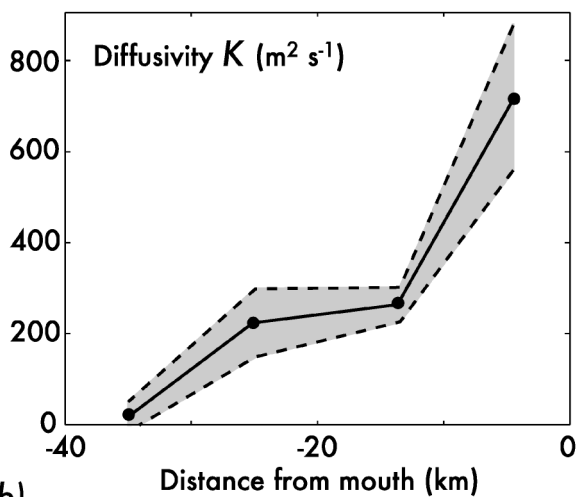
b. Signal penetration and propagation speed

A constant K is only a satisfactory parameterization of up-estuary salt flux in low-flow conditions if it reproduces both the propagation rate and penetration distance observed for ocean signals. To derive predictions of these parameters from the axial profile of K calculated above, we numerically integrated the differential form of (4.1)

$$a \frac{\partial \bar{s}}{\partial t} = \frac{\partial}{\partial x} \left(a K \frac{\partial \bar{s}}{\partial x} \right), \quad (4.2)$$



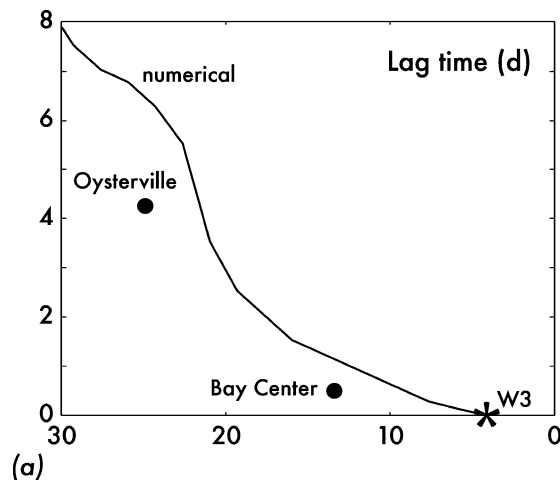
(a)



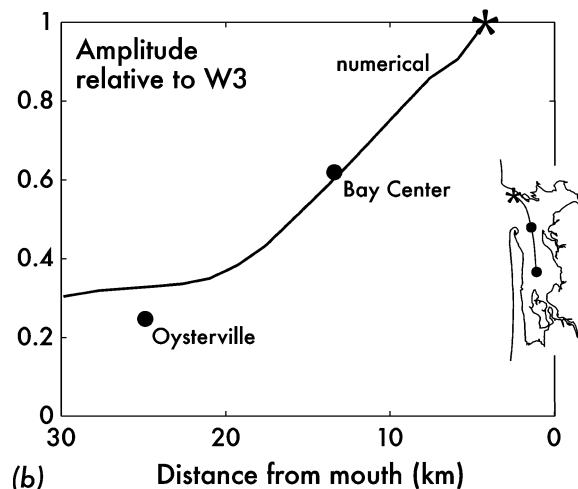
(b)

FIG. 6. (a) Time-change term vs axial salinity gradient at each Stanley Channel station, in low-flow conditions. The slope of the regressions (solid lines) is the diffusivity K . (b) Diffusivities from (a) shown as an along-channel profile. Dashed lines give 95% confidence limits on the slope.

using a simple forward-in-time, centered-in-space scheme, with data from W3 supplying the seaward boundary condition. Numerical results cannot be compared point-by-point with station salinities, both because of the neglected exchanges between Stanley Channel and the other subestuaries, and because even $\sim 10\%$ biases in $\partial\bar{s}/\partial t$ (see section 3b) quickly become $O(1)$ errors in the time-integral. Instead, to isolate up-



(a)



(b)

FIG. 7. (a) Lag times in days relative to W3 and (b) relative amplitude of the part of the signal correlated with W3, for detrended salinity data from Jul–Sep 1999 (dots) and a numerical solution to (4.2) for the same time period (lines).

stream-propagating signals, we calculate lag times of maximum correlation with W3 and amplitude of the correlated part of the signal (i.e., slope between salinity at each station and at W3). Results are shown in Fig. 7 for the low-flow period July–September 1999, and the reach of Stanley Channel from the mouth to Oysterville. Naselle and the small volume at the head of the channel, where signal penetration is weak and K is poorly constrained, are omitted.

The numerical solution follows the empirical pattern with reasonable accuracy, and reproduces, qualitatively, the rapid propagation of signals to Bay Center and the abrupt slowdown between Bay Center and Oysterville. Note that the propagation rate and penetration distance of ocean signals depend as much on the frequency of the boundary forcing as on the internal dynamics of the estuary. If single-frequency forcing is used in place of data from W3, (4.2) becomes the classical oscillatory boundary layer problem (Batchelor 1967, p. 353ff), and

the numerical solution reproduces the expected relationships among propagation rate, penetration distance, and forcing frequency.

c. Dynamics of “diffusion”

What physical meaning can be given to the magnitude of K , and to its 30-fold decrease over the length of Stanley Channel (Fig. 6)? We wrote above that K represents a combination of tide-, wind-, and ocean-density-driven mechanisms. Hickey et al. (2002) find that the distribution of residual currents in Willapa suggests tide- and density-driven circulations more than local-wind-driven circulations: we cannot quantify the local wind contribution more than this with available data, but we can guess that it does not set the scale of K . This leaves tidal and baroclinic mechanisms and the coupling between them.

Zimmerman (1986) offers two models to explain the large (100–1000 $\text{m}^2 \text{s}^{-1}$) diffusivities commonly observed in tidal waters. The first consists of a cascade of turbulent processes, in which lateral shears amplify dispersion by vertical shears, which in turn amplify dispersion by small-scale turbulence proper. The second relies on lateral shears alone. He proposes dispersion by “Lagrangian chaos,” in which the tidally averaged flow field is deterministic and steady but spatially complex—randomized by bathymetry rather than by turbulence—so that Lagrangian trajectories through that flow field are strongly divergent. Complex tidal-residual flow fields are often observed (Kuo et al. 1990; Li and O’Donnell 1997; Blanton and Andrade 2001) and the divergence of trajectories in a such a field is clear from simulation (Ridderinkhof and Zimmerman 1992). The open question is how commonly this type of density-independent tidal dispersion dominates over baroclinic mechanisms, or interactions between tidal and baroclinic mechanisms (Smith 1996; Valle-Levinson and O’Donnell 1996), in estuaries with measurable stratification.

In the remainder of this section we will verify the consistency of the simplest possibility for Willapa’s low-flow period dynamics: that the bathymetric tidal-residual field alone sets the scale of K in the long-term average, even if the dynamics of individual events are partly baroclinic or wind-driven. We hypothesize then that K scales with the amplitude and width of the largest residual eddies (MacCready 1999). Since in Willapa the tidal excursion is greater than the width of the estuary, this model implies

$$K \approx c_K U_T b, \tag{4.3}$$

where c_K is a constant of proportionality $O(1)$ or smaller, U_T is the rms tidal velocity, and b is the channel width. The empirical values of K calculated in section 4a are shown as a function of $U_T b$ in Fig. 8. We calculate b as cross-sectional area divided by mean depth below mean sea level. Among the four stations c_K varies be-

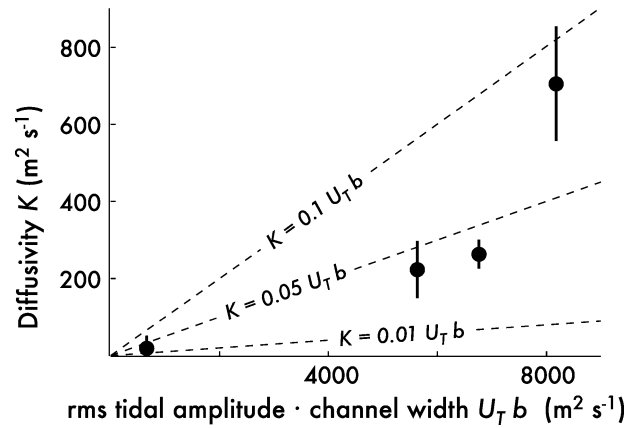


FIG. 8. Diffusivities from Fig. 6 compared with the product of tidal velocity and channel width. The predicted scaling (4.3) is shown for three values of c_K .

tween 0.03 and 0.09: if residual velocities are 10%–20% of the rms tidal amplitude as Zimmerman (1986) suggests is generally true and residual eddies are roughly one-half of the width of the estuary, we would expect $c_K = 0.05$ – 0.1 . The conceptual model behind (4.3) is thus consistent. Since U_T varies only fractionally over the length of Stanley Channel and b varies by a factor of 9, this correlation primarily tests the dependence of K on b .

We can test the dependence of K on U_T by indirect means. The scaling (4.3) predicts that K increases linearly with tidal velocity, so that the rate of up-estuary salt flux should be greater on spring tides than on neap tides. This prediction is contrary to the expectation for baroclinic exchange flows, which typically are retarded by spring tides because of increased vertical mixing (e.g., Park and Kuo 1996). Propagation rates between W3 and Oysterville are shown in Fig. 9 for 12 events during the July–September 1999 period considered above. The trend with tidal height (a proxy for tidal velocity) is positive and close to linear, as expected for tidally driven, rather than tidally inhibited, exchange.

As a final consistency check on our tidal-residual model of exchange, we can associate K with a net volume flux through the estuary mouth: if this volume flux is tidally driven, it should not exceed one tidal prism per tidal cycle. In general we can write

$$K \frac{\partial \bar{s}}{\partial x} = \frac{q}{a} \Delta s_{\text{in-out}}, \tag{4.4}$$

where q is the net subtidal volume flux and $\Delta s_{\text{in-out}}$ is the salinity difference between incoming and outgoing flows. For the case of Willapa we can guess that the axial salinity variation over one tidal excursion L_T is the largest variation upon which lateral shears can act: $\Delta s_{\text{in-out}} \leq L_T (\partial \bar{s} / \partial x)$. This condition is consistent with the differential-advection mechanism described by O’Donnell (1993) and others, and observed in Willapa by Hickey and Banas (2003). Equation (4.4) thus becomes

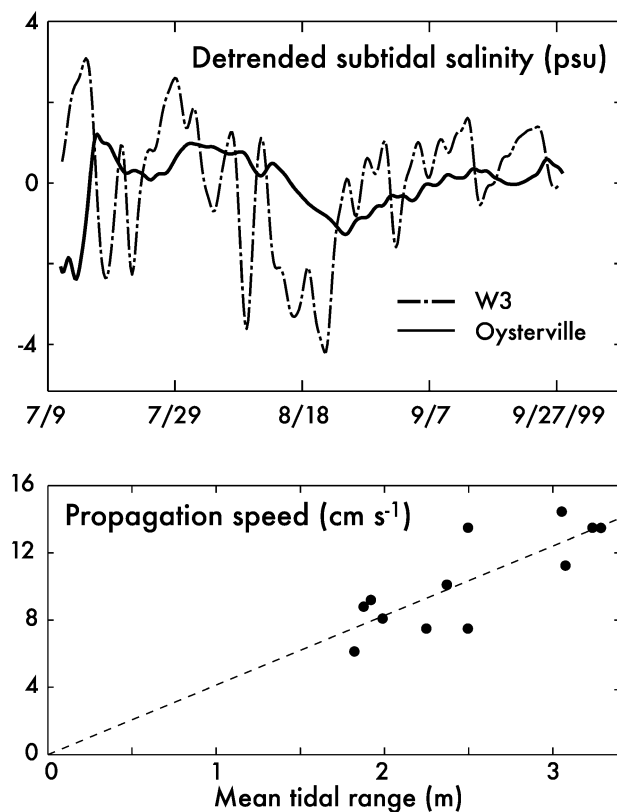


FIG. 9. (a) Detrended subtidal salinity at W3 and Oysterville, Jul–Sep 1999. (b) Signal propagation rate, inferred from the lagged correlation between W3 and Oysterville for individual maxima and minima in the record shown in (a) regressed to tidal amplitude.

$$q \geq \frac{aK}{L_T}. \quad (4.5)$$

The right-hand side is roughly $3000 \text{ m}^3 \text{ s}^{-1}$ at W3, whereas Willapa's total tidal volume flux is roughly $10\,000 \text{ m}^3 \text{ s}^{-1}$ (NOAA/EPA 1991). Willapa's tidal exchange ratio—the fraction of the tidal prism replaced by new water on the following tide—thus is ≥ 0.3 , consistent with the range of typical values reported by Dyer (1973). Note that as a and K decrease landward, so may the tidal exchange ratio.

5. Discussion and conclusions

a. Tide-driven exchange

To summarize the results of the previous section: during low-flow conditions, at all stations, the effective diffusivity K scales as 10%–20% of the tidal velocity times the channel width. This diffusion process appears on average to be tidally driven, not tidally damped (Fig. 9), although the up-estuary propagation of individual upwelling–downwelling pulses is known to have a baroclinic component as well (Hickey et al. 2002). This tidal exchange mechanism is very efficient near the mouth, replacing a minimum of 30% of the tidal prism—that

is, 15% of the bay volume (Hickey and Banas 2003)—every tidal cycle.

We speculate that strong along-coast currents on the inner shelf (Hickey 1989) may partly explain this efficiency, if they tend to advect each ebb tidal prism out of the reach of the following flood. We speculate also that the strength of tidal stirring on this coast may be increased by the fact that where East Coast estuaries have high and channelized intertidal salt marshes, Pacific Northwest estuaries generally have broad, deep sand or mud flats (Emmett et al. 2000).

b. A parameter space for unsteady estuaries

The results discussed in section 3 imply that this tidal exchange mechanism is important not just in low-flow conditions, but in fact in all seasons, even at high flows when stratification is several practical salinity units (Fig. 4). To summarize the relationships between tide- and river-driven exchange and the unsteadiness of the salt balance, we can rearrange Fig. 5 and (3.12) into a simple and general diagnostic scheme.

We begin by scaling the full, unsteady salt balance (3.11) by the river term:

$$\frac{l_a \frac{\partial \bar{s}}{\partial t}}{\frac{Q}{\bar{s}}} + 1 = \frac{K_{gc} \frac{\partial \bar{s}}{\partial x}}{\frac{Q}{\bar{s}}} + \frac{K \frac{\partial \bar{s}}{\partial x}}{\frac{Q}{\bar{s}}}. \quad (5.1)$$

We will call the first term in (5.1) the *unsteadiness* ψ : when $\psi > 0$, the estuary gains salt and when $\psi < 0$ it loses it. When $\psi = -1$, all the salt flushed by the river is lost, and the net up-estuary flux (the right-hand side) is 0. The two terms on the right-hand side can be called *scaled gravitational circulation* and *scaled diffusion*. The relationship between them is described by the parameter ν , the diffusive fraction of up-estuary salt flux, just as in the HR66 balance:

$$\nu \equiv \frac{K}{K_{gc} + K}. \quad (5.2)$$

We thus have two diagnostic parameters, ν and ψ , which specify the dominant balance in (3.11) or (5.1) just as ν alone diagnoses the steady HR66 balance.

Plotting scaled diffusion against scaled gravitation circulation creates a convenient parameter space (Fig. 10a), in which contours of ν sweep across the first quadrant and contours of ψ form a set of parallel diagonals. The first quadrant can be divided into three regimes, illustrated in Fig. 10a: the $\psi > 0, \nu > 0.5$ region, in which the estuary gains salt primarily through diffusion; the $\psi > 0, \nu < 0.5$ region, in which the estuary gains salt primarily through the gravitational circulation; and the $\psi < 0$ region, in which the river-flushing term dominates, and the estuary loses salt. The third quadrant, in which $\psi < -1$ and the “up estuary” fluxes are negative, represents reversals of the axial gradient in which dif-

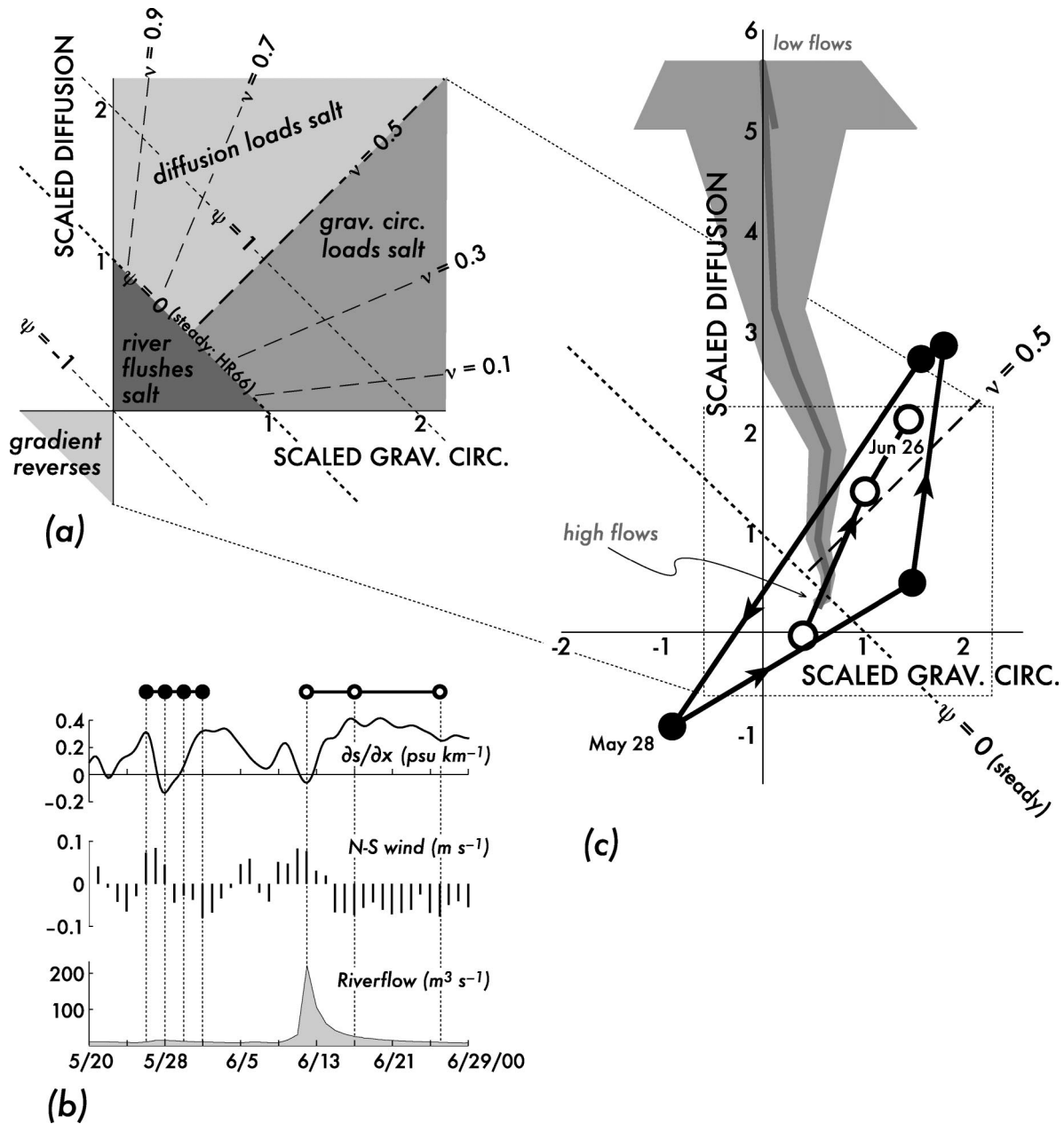


FIG. 10. (a) Diagnostic parameter space defined by terms in the scaled unsteady salt balance (5.1). The axis variables are the diffusion and gravitational-circulation terms scaled by the river term; ψ is the unsteadiness parameter, and ν is the diffusive fraction of up-estuary salt flux (see section 5b). Dynamical regimes are labeled and shaded. (b) Expanded time series of meteorological forcing and axial salinity gradient for the spring 2000 period indicated in Fig. 4. Two events, each a connected series of instantaneous observations, are indicated; the solid and open circles are keys to (c). (c) Seasonal and event-scale results from Bay Center plotted in the parameter space shown in (a). Only the dynamical regime-defining contours $\psi = 0$ and $\nu = 0.5$ are repeated from (a). The riverflow-averaged results shown in Fig. 5 are plotted here as a thick gray line; the low-flow and high-flow ends of this line are indicated. Solid and open connected circles show Willapa's trajectory through the events shown in (b). Note that the final snapshot on 26 Jun corresponds to the main-channel transect shown in Fig. 3g.

fusion and gravitational circulation actively move salt seaward. (The second and fourth quadrants represent reversals in one but not both of these mechanisms, scenarios which seem unlikely in nature.)

To place the riverflow-ensemble-average results from

section 3c on this diagram, we can rewrite the scaled-gravitational-circulation and scaled-diffusion terms using (3.9): they become $K_{gc}(K_{tot}^{eq})^{-1}$ and $K(K_{tot}^{eq})^{-1}$, respectively. Note that scaling $\partial\bar{s}/\partial x$ out of these terms in this way maps axial gradient reversals, which should

appear in the third quadrant, onto the first. Results for Bay Center are shown in Fig. 10c: these are simply a more succinct rearrangement of the results shown in Fig. 5. At low flows, the estuary is far into the “diffusion loads salt” regime: $\psi \gg 1$ and v is close to 1. At high flows, the estuary enters the “river flushes salt” regime.

We can place individual events in this parameter space—very tentatively, given the limitations of the dataset—for comparison with the riverflow-ensemble-average results. Time series of wind, riverflow, and $\partial\bar{s}/\partial x$ from spring 2000 are shown in Fig. 10b. Two events are indicated. In the first (solid circles), a short period of northward (downwelling favorable) winds forces an axial gradient reversal, likely an intrusion of the Columbia plume. In the second (open circles), another period of northward wind accompanies a strong peak in local riverflow. Subtidal snapshots of conditions at Bay Center during these events, from the initial response through the relaxation back to upwelling conditions, are shown in Fig. 10c. The gravitational term has been calculated, for lack of a better option, as the difference between the other terms in (5.1), so that points in the parameter space are determined by ψ and the vertical coordinate. The diffusion term has been calculated using the long-term mean K ; the scatter in Fig. 6 suggests that the errors here may well be $O(1)$, and so we will interpret these results only qualitatively.

The bay’s trajectory during the second, river-forced event follows the riverflow-averaged pattern: river-flushing dominates during the flow peak itself, but the estuary returns to diffusive salt loading, typical low-flow-period dynamics, over a few weeks. During the first event, the estuary cycles from diffusive salt-loading to strong salt flushing and back over only 8 days. Note that during the gradient reversal the rate of salt flushing is several times larger than the river term ($\psi \approx -2.5$ on 28 May; Fig. 10c). These trajectories thus illustrate not only Willapa’s changeability on the event scale, but also the power of oceanic water-property variations to force transient fluxes through an estuary several times stronger than the steady, river-driven fluxes usually emphasized in estuarine classification.

c. Generalizing to other unsteady systems

The extreme unsteadiness of the salt balance in Willapa—imbalances not just on the same scale as the river-driven fluxes, but many times larger—appear to result from the combination of highly variable ocean forcing with dispersion mechanisms strong enough to propagate these forcing fluctuations far upstream on their time scale of variation. Even in the absence of strong ocean variability, however, variations in riverflow may still drive $O(1)$ imbalances in the salt budget. Simpson et al. (2001) found a seasonal pattern very similar to Willapa’s in the Conwy in Wales, where tidal upstream salt flux greatly exceeds downstream river-driven flux for all except occasional high-riverflow events.

A common formalism (e.g., HR65; Kranenburg 1986) invites us to think of the estuarine salt budget as the sum of a steady balance like (3.5) and transient processes, and then to define an averaging timescale, the “adjustment time,” above which the transients are negligible. (HR65 implicitly takes the tidal period as the adjustment time.) This formalism is not germane to an estuary as strongly forced as Willapa or the Conwy, where the salt balance is only close to steady in averages so long (1 yr or perhaps longer; section 3c) that they do not allow us to distinguish one forcing regime from another. Accordingly, in section 5b we have proposed a formalism in which the unsteadiness of the salt balance enters as part of the basis for estuarine description and classification, rather than entering only as noise.

Acknowledgments. This work was supported by grants NA76 RG0119 Project R/ES-9, NA76 RG0119 AM08 Project R/ES-33, NA16 RG1044 Project R/ES-42, NA76 RG0485 Project R/R-1, and NA96 OP0238 Project R/R-1 from the National Oceanic and Atmospheric Administration to Washington Sea Grant Program, University of Washington, and by Grant CR 824472-01-0 from the Environmental Protection Agency. NSB was also supported by a National Defense Science and Engineering Graduate fellowship. Bill Fredericks, Jim Johnson, and Sue Geier at the University of Washington, and Eric Siegel, Kara Nakata, Julia Bos, and Casey Clishe at the Washington Department of Ecology were responsible for data collection and initial processing. Many thanks are given to Brett Dumbauld and the Washington Department of Fish and Wildlife for their generous logistical support. Conversations with Stephen Monismith were very helpful.

REFERENCES

- Andrews, R. S., 1965: Modern sediments of Willapa Bay, Washington: A coastal plain estuary. University of Washington Department of Oceanography Tech. Rep. 118, 48 pp.
- Batchelor, G. K., 1967: *An Introduction to Fluid Dynamics*. Cambridge University Press, 615 pp.
- Blanton, J. O., and F. A. Andrade, 2001: Distortion of tidal currents and the lateral transfer of salt in a shallow coastal plain estuary (O Estuario do Mira, Portugal). *Estuaries*, **24**, 467–480.
- Bowden, K. F., and R. M. Gilligan, 1971: Characterisation of features of estuarine circulation as represented in the Mersey Estuary. *Limnol. Oceanogr.*, **16**, 490–502.
- Dronkers, J., and J. van de Kreeke, 1986: Experimental determination of salt intrusion mechanisms in the Volkerak estuary. *Neth. J. Sea Res.*, **20**, 1–19.
- Duxbury, A. C., 1979: Upwelling and estuary flushing. *Limnol. Oceanogr.*, **24**, 627–633.
- Dyer, K. R., 1973: *Estuaries: A Physical Introduction*. John Wiley and Sons, 140 pp.
- Emmett, R., and Coauthors, 2000: Geographic signatures of North American West Coast estuaries. *Estuaries*, **23**, 765–792.
- Fischer, H. B., 1976: Mixing and dispersion in estuaries. *Annu. Rev. Fluid Mech.*, **8**, 107–133.
- Geyer, W. R., 1997: Influence of wind on dynamics and flushing of shallow estuaries. *Estuarine Coastal Shelf Sci.*, **44**, 713–722.
- Gibson, J. R., and R. G. Najjar, 2000: The response of Chesapeake

- Bay salinity to climate-induced changes in streamflow. *Limnol. Oceanogr.*, **45**, 1764–1772.
- Hansen, D. V., and M. Rattray Jr., 1965: Gravitational circulation in straits and estuaries. *J. Mar. Res.*, **23**, 104–122.
- , and —, 1966: New dimensions in estuary classification. *Limnol. Oceanogr.*, **11**, 319–326.
- Hickey, B. M., 1989: Patterns and processes of circulation over the shelf and slope. *Coastal Oceanography of Washington and Oregon*, B. M. Hickey and M. R. Landry, Eds., Elsevier, 41–115.
- , and N. S. Banas, 2003: Oceanography of the U.S. Pacific Northwest coastal ocean and estuaries with application to coastal ecology. *Estuaries*, **26**, 1010–1031.
- , X. Zhang, and N. Banas, 2002: Coupling between the California Current System and a coastal plain estuary in low riverflow conditions. *J. Geophys. Res.*, **107**, 3166, 10.1029/1999JC000160.
- Hughes, R. P., and M. Rattray, 1980: Salt flux and mixing in the Columbia River Estuary. *Estuarine Coastal Mar. Sci.*, **10**, 479–494.
- Jay, D. A., and J. D. Smith, 1988: Residual circulation in and classification of shallow, stratified estuaries. *Physical Processes in Estuaries*, J. Dronkers and W. van Leussen, Eds., Springer-Verlag, 21–41.
- , and —, 1990: Residual circulation in shallow, stratified estuaries. Part II: Weakly-stratified and partially-mixed systems. *J. Geophys. Res.*, **95**, 733–748.
- Kalnay, E., and Coauthors, 1996: The NCEP/NCAR 40-Year Reanalysis Project. *Bull. Amer. Meteor. Soc.*, **77**, 437–471.
- Kjerfve, B., 1986: Circulation and salt flux in a well mixed estuary. *Physics of Shallow Estuaries and Bays*, J. van de Kreeke, Ed., Springer-Verlag, 22–29.
- Kranenburg, C., 1986: A timescale for long-term salt intrusion in well-mixed estuaries. *J. Phys. Oceanogr.*, **16**, 1329–1331.
- Kraus, N. C., Ed., 2000: *Study of Navigation Channel Feasibility, Willapa Bay, Washington*. U.S. Army Engineer District Final Report, 440 pp.
- Kuo, A. Y., J. M. Hamrick, and G. M. Sisson, 1990: Persistence of residual currents in the James River estuary and its implication to mass transport. *Residual Currents and Long-Term Transport*, R. T. Cheng, Ed., Springer-Verlag, 389–401.
- Lewis, R. E., and J. O. Lewis, 1983: The principal factors contributing to the flux of salt in a narrow, partially stratified estuary. *Estuarine Coastal Shelf Sci.*, **33**, 599–626.
- , and R. J. Uncles, 2003: Factors affecting longitudinal dispersion in estuaries of different scale. *Ocean Dyn.*, **53**, 197–207.
- Li, C., and J. O'Donnell, 1997: Tidally induced residual circulation in shallow estuaries with lateral depth variation. *J. Geophys. Res.*, **102**, 27 915–27 929.
- Lincoln, J. H., 1977: Derivation of freshwater inflow into Puget Sound. University of Washington Department of Oceanography Special Rep. 72, 20 pp.
- Linden, P. F., and J. E. Simpson, 1988: Modulated mixing and frontogenesis in shallow seas and estuaries. *Cont. Shelf Res.*, **8**, 1107–1127.
- MacCready, P., 1999: Estuarine adjustment to changes in river flow and tidal mixing. *J. Phys. Oceanogr.*, **29**, 708–726.
- McCarthy, R. K., 1993: Residual currents in tidally dominated, well-mixed estuaries. *Tellus*, **45A**, 325–340.
- Monismith, S. G., W. Kimmerer, J. R. Burau, and M. T. Stacey, 2002: Structure and flow-induced variability of the subtidal salinity field in northern San Francisco Bay. *J. Phys. Oceanogr.*, **32**, 3003–3019.
- Monteiro, P. M. S., and J. L. Largier, 1999: Thermal stratification in Saldhana Bay (South Africa) and subtidal, density-driven exchange with the coastal waters of the Benguela Upwelling System. *Estuarine Coastal Shelf Sci.*, **49**, 877–890.
- NOAA/EPA, 1991: Susceptibility and status of West Coast estuaries to nutrient discharges: San Diego Bay to Puget Sound. Summary Report, Strategic Assessment of Near Coastal Waters, 35 pp.
- O'Donnell, J., 1993: Surface fronts in estuaries: A review. *Estuaries*, **16**, 12–39.
- Officer, C. B., and D. R. Kester, 1991: On estimating the non-advective tidal exchanges and advective gravitational circulation exchanges in an estuary. *Estuarine Coastal Shelf Sci.*, **32**, 99–103.
- Park, K., and A. Y. Kuo, 1996: Effect of variation in vertical mixing on residual circulation in narrow, weakly nonlinear estuaries. *Buoyancy Effects on Coastal and Estuarine Dynamics*, D. G. Aubrey and C. T. Friedrichs, Eds., Amer. Geophys. Union, 301–317.
- Pritchard, D. W., and R. E. Bunce, 1959: Physical and chemical hydrography of the Magothy River. Chesapeake Bay Institute Tech. Rep. XVII, Ref. 59–2.
- , and J. H. Carpenter, 1960: Measurements of turbulent diffusion in estuarine and inshore waters. *Bull. Int. Assoc. Sci. Hydrol.*, **20**, 37–50.
- Ridderinkhof, H., and J. T. F. Zimmerman, 1992: Chaotic stirring in a tidal system. *Science*, **258**, 1107–1111.
- Roegner, G. C., B. M. Hickey, J. A. Newton, A. L. Shanks, and D. A. Armstrong, 2002: Wind-induced plume and bloom intrusions into Willapa Bay, Washington. *Limnol. Oceanogr.*, **47**, 1033–1042.
- Schroeder, W. W., S. P. Dinnel, and W. J. Wiseman Jr., 1992: Salinity structure of a shallow, tributary estuary. *Dynamics and Exchanges in the Coastal Zone*, D. Prandle, Ed., Amer. Geophys. Union, 155–171.
- Simpson, J. H., R. Vennell, and A. J. Souza, 2001: The salt fluxes in a tidally-energetic estuary. *Estuarine Coastal Shelf Sci.*, **52**, 131–142.
- Smith, R., 1996: Combined effects of buoyancy and tides upon longitudinal dispersion. *Buoyancy Effects on Coastal and Estuarine Dynamics*, D. G. Aubrey and C. T. Friedrichs, Eds., Amer. Geophys. Union, 319–330.
- Stacey, M. T., J. R. Burau, and S. G. Monismith, 2001: Creation of residual flows in a partially stratified estuary. *J. Geophys. Res.*, **106**, 17 013–17 037.
- Uncles, R. J., and J. A. Stephens, 1990: Computed and observed currents, elevations, and salinity in a branching estuary. *Estuaries*, **13**, 133–144.
- , and D. H. Peterson, 1996: The long-term salinity field in San Francisco Bay. *Cont. Shelf Res.*, **16**, 2005–2039.
- Valle-Levinson, A., and J. O'Donnell, 1996: Tidal interaction with buoyancy driven flow in a coastal-plain estuary. *Buoyancy Effects on Coastal and Estuarine Dynamics*, D. G. Aubrey and C. T. Friedrichs, Eds., Amer. Geophys. Union, 265–281.
- Walters, R. A., 1982: Low-frequency variations in sea level and currents in south San Francisco Bay. *J. Phys. Oceanogr.*, **12**, 658–668.
- Wang, D.-P., and A. J. Elliot, 1978: Nontidal variability in the Chesapeake Bay and Potomac River: Evidence for nonlocal forcing. *J. Phys. Oceanogr.*, **8**, 225–232.
- Wang, J., R. T. Cheng, and P. C. Smith, 1997: Seasonal sea-level variations in San Francisco Bay in response to atmospheric forcing, 1980. *Estuarine Coastal Shelf Sci.*, **45**, 39–52.
- Winterwerp, J. C., 1983: The decomposition of mass transport in narrow estuaries. *Estuarine Coastal Mar. Sci.*, **16**, 627–639.
- Wiseman, W. J., Jr., E. M. Swenson, and F. J. Kelly, 1990: Control of estuarine salinities by coastal ocean salinity. *Residual Currents and Long-Term Transport*, R. T. Cheng, Ed., Springer-Verlag, 184–193.
- Wong, K.-C., and X. Lu, 1994: Low-frequency variability in Delaware's inland bays. *J. Geophys. Res.*, **99**, 12 683–12 695.
- , and J. E. Moses-Hall, 1998: On the relative importance of the remote and local wind effects to the subtidal variability in a coastal plain estuary. *J. Geophys. Res.*, **103**, 18 393–18 404.
- Zimmerman, J. T. F., 1976: Mixing and flushing of tidal embayments in the western Dutch Wadden Sea, Part I: Distribution of salinity and calculation of mixing time scales. *Neth. J. Sea Res.*, **10**, 149–191.
- , 1986: The tidal whirlpool: A review of horizontal dispersion by tidal and residual currents. *Neth. J. Sea Res.*, **20**, 133–154.